ISSN 1063-7834, Physics of the Solid State, 2006, Vol. 48, No. 2, pp. 207–212. © Pleiades Publishing, Inc., 2006.
Original Russian Text © D.A. Balaev, I.L. Belozerova, D.M. Gokhfeld, L.V. Kashkina, Yu.I. Kuzmin, C.R. Michel, M.I. Petrov, S.I. Popkov, K.A. Shaikhutdinov, 2006, published in Fizika Tverdogo Tela, 2006, Vol. 48, No. 2, pp. 193–198.

METALS AND SUPERCONDUCTORS

Current–Voltage Characteristics of a Foamed $Bi_{1.8}Pb_{0.3}Sr_2Ca_2Cu_3O_x$ High-Temperature Superconductor with Fractal Cluster Structure

D. A. Balaev[1], I. L. Belozerova[2], D. M. Gokhfeld[1], L. V. Kashkina[3], Yu. I. Kuzmin[4], C. R. Michel[5], M. I. Petrov[1], S. I. Popkov[1, 2], and K. A. Shaikhutdinov[1]

[1]*Kirensky Institute of Physics, Siberian Division, Russian Academy of Sciences, Akademgorodok, Krasnoyarsk, 660036 Russia*
e-mail: smp@iph.krasn.ru
[2]*Reshetnev Siberian State Aerospace University, Krasnoyarsk, 660014 Russia*
[3]*Krasnoyarsk State University, Krasnoyarsk, 660041 Russia*
[4]*Ioffe Physicotechnical Institute, Russian Academy of Sciences, Politechnicheskaya ul. 26, St. Petersburg, 194021 Russia*
e-mail: yurk@mail.ioffe.ru
[5]*CUCEI Universidad de Guadalajara, Guadalajara, Jalisco, 44430 Mexico*

Received April 28, 2005

Abstract—The influence of the structure of foamed polycrystalline bismuth-based superconductors on their critical currents and current–voltage characteristics is studied. It is found that superconducting foams have a fractal structure, and the fractal dimension of the boundary between the normal and superconducting phases is estimated. The magnetic and transport properties of superconducting foams are investigated, and the current–voltage characteristics are obtained in a wide range of currents. The effect of percolation phenomena on vortex pinning in a foamed superconductor is considered. The current–voltage characteristics of the superconducting foams at the beginning of the resistive transition are found to be in good agreement with a model in which a magnetic flux is assumed to be trapped in the fractal clusters of a normal phase.

PACS numbers: 74.72.Hs, 74.81.Bd, 74.25.Fy, 61.43.Hv

DOI: 10.1134/S1063783406020016

1. INTRODUCTION

The recently discovered superconducting foams [1, 2] are superconducting materials of a new kind which have interesting physical properties [3–5]. A foamed superconductor is a percolation system in which there are an infinite superconducting cluster conducting a transport current and pores of different shape, both closed and open. Pores also form clusters. In a certain range of material densities, the infinite superconducting cluster can coexist with the infinite cluster of open pores. Such a system gives an interesting example of polychromatic percolation [6], where the percolation of an electric current along a superconducting cluster and the percolation of a magnetic flux penetrating into a pore cluster proceed concurrently. An essential problem regarding the magnetic and transport properties of superconducting foams is how the topology of an infinite cluster, which is a multiply connected superconducting region, affects the pinning and transport of vortices. From the practical point of view, it is important that superconducting foams have a high specific surface area to provide effective heat removal by a cooling agent (liquid nitrogen or helium), which penetrates into open pores. This feature, as well as the still not fully understood peculiarity of the vortex pinning and transport [4, 5], allows foamed high-temperature superconductors (HTS) to have high magnetic critical currents that make these materials promising for practical applications.

2. FRACTAL STRUCTURE OF SUPERCONDUCTING FOAMS

Low-density samples of $Bi_{1.8}Pb_{0.3}Sr_2Ca_2Cu_3O_x$ (BPSCCO) were produced through solid-phase synthesis. The synthesis was about 400 h long. We used technology similar to that described in [7] but with the final annealing conditions modified in such a way that they favored the growth of superconductor microcrystallites along the *ab* plane. As a result of random crystallite orientation, such a growth process leads to material bulking. Another specific feature of the synthesis technique used is that the calcium-deficient precursor was supplied with calcium carbonate, which ultimately decomposed during the final annealing. The excess pressure of

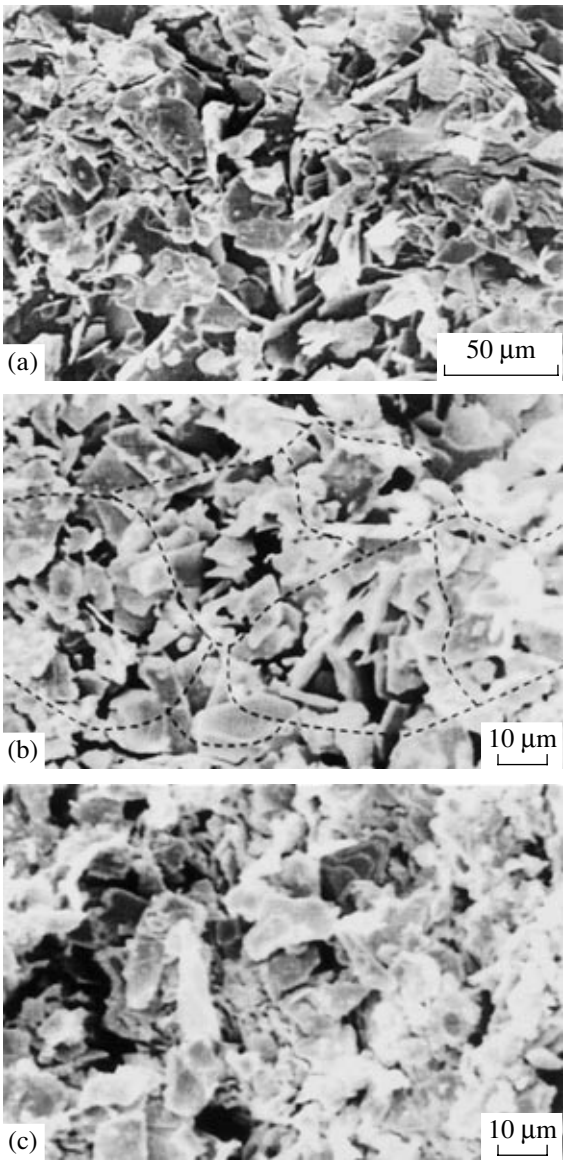

Fig. 1. SEM images of three different cleavages of a sample of BPSCCO superconducting foam. The micrographs are taken at a magnification of (a) 500 and (b, c) 1000. The dash lines in panel (b) show possible current paths in an infinite superconducting cluster.

the resulting carbon dioxide also contributed to the sample bulking.

The microphotographs of three natural cleavage surfaces of a foamed BPSCCO obtained using a scanning electron microscope (SEM) are shown in Fig. 1. The SEM images of many natural cleavages of different samples were very similar. The density of the material obtained was 2.26 g/cm^3, which is about 38% of the maximum density of monolithic BPSCCO ceramics. The volume ratio of the superconducting phase exceeded the percolation threshold, so the percolation cluster was dense enough. Since BPSCCO microcrystallites have a platelike shape, a bismuth-based superconducting foam has a specific flaky structure, which is much more ramified than that of YBCO-based foams (see photos in [2, 4]). The SEM images shown in Fig. 1 confirm the existence of a three-dimensional percolation superconducting cluster in superconducting BPSCCO foams. Possible percolation paths are shown in Fig. 1b. The superconducting cluster is a conglomeration of randomly oriented BPSCCO microcrystallites, which have the shape of a plate and are 10- to 20-μm wide and 1- to 2-μm thick. Pores between crystallite clusters are also clearly seen in Fig. 1.

Since the boundary between the superconducting and normal phases is strongly ramified (Fig. 1), it is reasonable to expect that there will be fractal clusters in superconducting foams. Indeed, an analysis of microphotographs reveals a fractal structure of clusters in foamed superconductors. In order to estimate the fractal dimension of the boundaries of the normal-phase clusters, the "box-counting" method was used with which the boundaries of the cluster cross sections seen in the electron microphotographs were studied.

SEM images of the superconducting foam cleavages (Fig. 1) were covered with square grids of $L \times L$ cells. The size of the grid cell was small enough (the values of L ranged from 75 to 1200 nm) for measuring all the bends of the microcrystallite boundaries. If a fractal curve (the part of the boundary of the cluster cross section by the image plane) goes in a square of side L_{max}, then each of its $N(L)$ self-similar subsets will go in a square of side $L = L_{max}/r$, where r is the scaling factor [8]. The minimum number of such squares of side L required to cover the explored part of the boundary is equal to

$$N(L) = r^D = \left(\frac{L_{max}}{L}\right)^D \propto L^{-D}, \quad (1)$$

where D is the fractal dimension [8]. It follows that the fractal dimension of the boundary between the superconducting and normal phases is given by

$$D = \frac{\ln N(L)}{\ln(L_{max}/L)}. \quad (2)$$

Obviously, D cannot exceed the topologic dimension of a plane, which is equal to 2.

The ratio between the size of the measuring cell L and the big square side L_{max} sets the unit of measurement of length. At $L_{max} = 1$, Eq. (2) for the fractal dimension becomes [9] $D = -\ln(N(L))/\ln(L)$.

Therefore, it is possible to find the fractal dimension of the cluster boundary by counting the number $N(L)$ of nonempty cells of area L^2 that covers a given part of the boundary. To attain an estimate of highest precision, we have to get a wide range of progressively smaller values of L and to average the obtained values of D over all the configurations. The simplest way to do that is to plot the $N(L)$ dependence on a log–log scale: according to Eq.

(1), the resulting curve has to be linear with a slope equal to the fractal dimension of the cluster boundary. We analyzed microphotographs of cleavage surfaces of BPSCCO foams obtained at magnifications of 500 and 1000. The size of the measuring cell was $L = 150$, 300, 600, and 1200 nm for the microphotographs with a magnification of 500 and $L = 75$, 150, 300, and 600 nm for the photos with a magnification of 1000. The results of the fractal dimension measurements are presented in Fig. 2. Points *a* are obtained by scanning and digital processing of the microscopic image shown in Fig. 1a, and points *b* and *c* correspond to the two other microscopic images shown in Figs. 1b and 1c, respectively. The $N(L)$ dependences for the different cleavages presented in Fig. 2 on a log–log scale are approximated well by straight lines (the correlation factor is 0.99), with their slopes being equal and corresponding to a fractal dimension $D = 1.80 \pm 0.06$. The found value of the fractal dimension differs substantially from unity, which means that the fractal properties of the cluster boundaries are really important. The dashed lines in Fig. 2 represent the limiting cases corresponding to the Euclid cluster boundaries ($D = 1$) and to fractal boundaries with a maximum fractal dimension ($D = 2$).

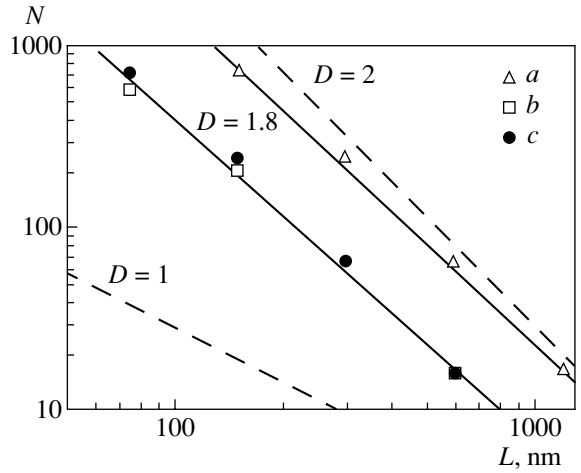

Fig. 2. Estimate of the fractal dimension of the boundaries between the normal and superconducting phases in a BPSCCO foam using (a) the SEM image shown in Fig. 1a (magnification 500) and (b, c) the SEM images shown in Figs. 1b and 1c (magnification 1000). The slopes of the dashed lines show the possible range for the fractal dimension from $D = 1$ for Euclidian boundaries to $D = 2$ for the maximum possible fractal dimension.

3. SUPERCONDUCTING PROPERTIES OF BPSCCO FOAMS

Current–voltage characteristics of the samples were measured using the standard four-probe technique in the dc current mode. Samples were manufactured in the shape of a parallelepiped $10 \times 4 \times 4$ mm in size, with their middle portion being ground down to 1–1.5 mm in thickness. The length of the thinned part was 6 mm. In order to produce contacts with small ohmic resistance, we baked an ultrafine silver powder into the region of current contacts of the sample. The resulting contact resistance does not exceed 10^{-4} Ω cm^2. We used pressure current and potential contacts made of a nonmagnetic gilded material. The distance between potential contacts was 5 mm. In order to improve heat exchange, the sample was immersed immediately into the cooling agent (liquid nitrogen or liquid helium) during measurements. The absence of self-heating is confirmed by the coincidence of the current–voltage characteristics recorded during direct and reverse current scanning at various rates. Magnetic measurements were performed using a vibrating-coil magnetometer with a superconducting solenoid [10]. Samples used for magnetic measurements had the shape of cylinders 0.5 mm in diameter and 4-mm long. A magnetic field was applied parallel to the sample axis.

The transition into the superconducting state in foamed BPSCCO occurs at 107 K (Fig. 3). The inset to Fig. 3 shows the magnetization curve for a sample measured at $T = 4.2$ K. For comparison, the inset also presents the magnetic-field dependence of the magnetization $M(H)$ for monolithic BPSCCO ceramics. The magnetization curves are similar in shape, but the

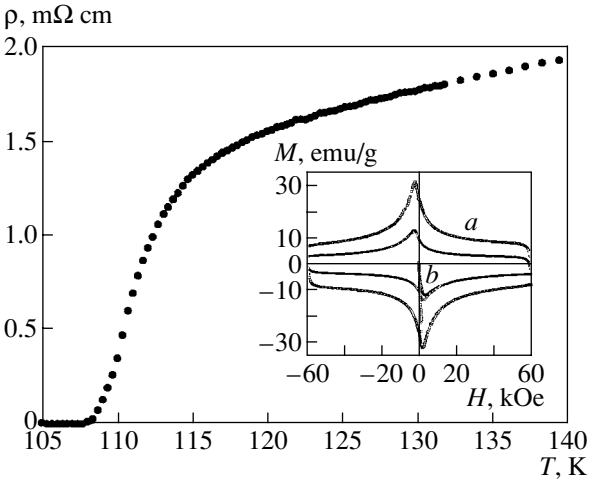

Fig. 3. Temperature dependence of the resistance of a BPSCCO superconducting foam. The inset shows the magnetization curves of BPSCCO (a) foam and (b) monolithic ceramics measured at $T = 4.2$ K.

diamagnetic response of the foamed material (expressed in emu/g) is 2.4 times larger than that of the monolithic material. Without normalization per mass (that is, for the same volume), the diamagnetic response of the superconducting foam exceeds that for the monolithic material by a factor of 1.6. The equivalent magnetic critical current of the foam found from the remanent magnetization using the Bean model is equal to 340 kA/cm^2 at $T = 4.2$ K, which is likewise 1.6 times larger than that for monolithic BPSCCO ceramics.

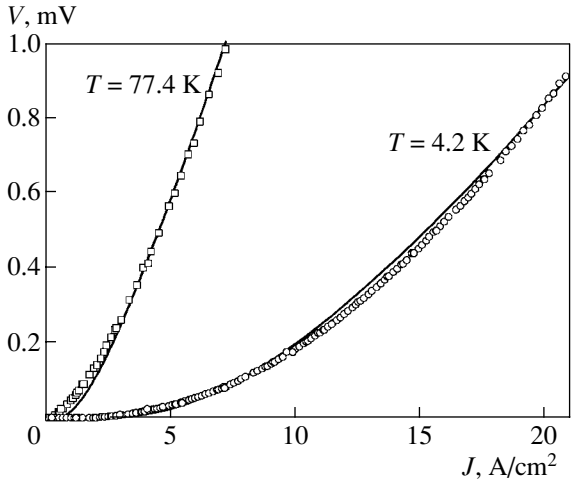

Fig. 4. Current–voltage characteristics of a BPSCCO superconducting foam. Points show experimental data obtained at liquid-helium and liquid-nitrogen temperatures, and solid lines are theoretical curves calculated for a fractal dimension of normal-phase cluster boundaries $D = 1.8$.

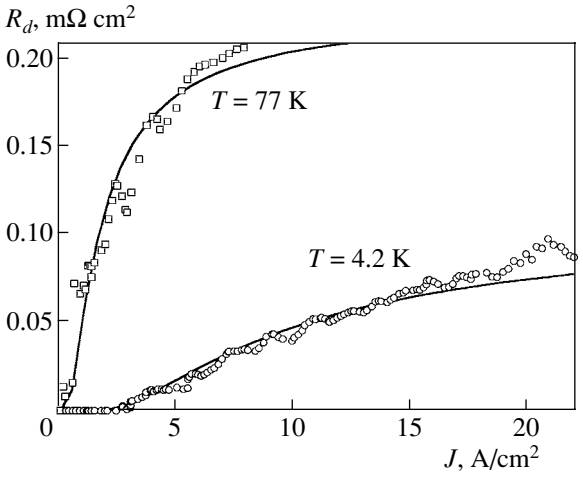

Fig. 5. Dependence of the differential resistance of a BPSCCO superconducting foam on current. Points show experimental data, and solid lines are theoretical curves calculated for a fractal dimension of normal-phase cluster boundaries $D = 1.8$.

The current–voltage characteristics of foamed BPSCCO at $T = 4.2$ and 77 K are shown in Fig. 4. The nonlinearity of these characteristics is an inherent feature of polycrystalline HTS. The dependences of the differential resistance on the transport current shown in Fig. 5 provide additional information on the vortex dynamics. The differential resistance is a low-signal parameter, which is most suitable for describing the nonlinear current–voltage characteristic of a superconductor. Study of current–voltage characteristics allows one to get new data concerning the nature of the vortex state in percolation materials [11, 12]. The region of the resistive transition is of special interest, primarily the initial part of the current–voltage characteristic, where a nonzero voltage drop appears, indicating the onset of dissipation. Here, vortices start to break away from pinning centers, a process which finally leads to the collapse of superconductivity. The motion of magnetic flux transferred by vortices induces an electric field and causes a dissipation of energy. In the case of HTS, the vortex motion is especially important because of the large thermal fluctuations and low pinning energies [11]. Superconductors containing isolated clusters of the normal phase provide strong pinning because the magnetic flux is trapped inside these clusters and cannot leave them without crossing the surrounding superconducting space. Such clusters consist of inclusions of the normal phase united by a common trapped flux and surrounded by the superconducting phase [13, 14]. When the current is increased, vortices start to break away from the clusters whose pinning force is smaller than the Lorentz force created by the transport current. Such a depinning has percolation nature [12, 15, 16], because the vortices move along random transport channels.

Clusters of the normal phase exert a significant effect on the dynamics of the trapped flux, especially when the clusters have fractal boundaries [14, 17]. In this case, the perimeter P and area A of a cluster cross section obey the scaling relation $P^{1/D} \propto A^{1/2}$ [8]. Fractal clusters are characterized by a very wide range of geometrical sizes of their structural features, into which the vortex diameter falls. This causes the clusters to strongly interact with vortices and efficiently capture the magnetic flux. Fractal clusters of the normal phase have been found in superconducting YBCO films [13]. The regime of fractal dissipation was observed in BSCCO and BPSCCO composite materials containing normal-phase inclusions of silver in bulk polycrystalline samples of YBCO and GdBCO [18]. The presence of fractal clusters in superconducting BPSCCO foams is confirmed by Fig. 2. Without an external magnetic bias (in the self-field regime), the magnetic flux is concentrated along closed irregular loops, which penetrate deeply into pores between the superconducting crystallites. In the course of depinning, the vortices have to overcome a barrier when they cross the boundary of the cross section of the normal-phase cluster by the plane where the current is flowing. The geometric properties of this boundary affect the dynamics of the trapped flux and, consequently, the current–voltage characteristic.

The influence of fractal clusters of the normal phase on the magnetic and transport properties of percolating superconductors was analyzed in [14, 17, 19, 20]. In those studies, the current–voltage characteristics of superconductors were calculated for various distributions of depinning currents and it was demonstrated that enhancement of pinning may be expected as the fractal dimension of normal-phase cluster boundaries increases. For exponential hyperbolic distributions of depinning currents, the current–voltage characteristic

of a superconductor containing fractal clusters of a normal phase is given by [20]

$$u = r_f\left[i\exp\left(-\left(\frac{2+D}{D}\right)^{2/D+1} i^{-2/D}\right) - \left(\frac{2+D}{D}\right)^{(2+D/2)} \times \Gamma\left(1-\frac{D}{2}, \left(\frac{2+D}{D}\right)^{2/D+1} i^{-2/D}\right)\right], \quad (3)$$

where u is the dimensionless voltage, r_f is the dimensionless flux flow resistance, $i = I/I_c$ is the dimensionless electric current normalized to the critical current of the transition into the resistive state I_c, and $\Gamma(\nu, z)$ is the complementary incomplete gamma function. The critical current of the transition into the resistive state I_c is determined as the point of intersection of the current axis and the tangent line drawn through the inflection point of the dependence of the differential resistance on the current. The critical current defined in such a way exceeds the critical current of the onset of dissipation, determined according to the "voltage criterion" as the current corresponding to a finite voltage induced by moving vortices. The dimensionless voltage u and the dimensionless flux flow resistance r_f are related to the corresponding dimensional values U and R_f by the relation $U/R_f = I_c(u/r_f)$.

Current–voltage characteristics found from Eq. (3) for the samples involved are shown in Fig. 4 (solid lines). We used the previously obtained value of the fractal dimension of the boundaries of normal-phase clusters. The critical current and the flux flow resistance were fitting parameters. Good agreement with the experimentally measured current–voltage characteristics in the region of the resistive transition is achieved with the following parameter values: $D = 1.8$, $J_c(4.2\ \text{K}) = 2.5\ \text{A/cm}^2$, $R_f(4.2\ \text{K}) = 0.11\ \text{m}\Omega\ \text{cm}^2$, $J_c(77\ \text{K}) = 0.4\ \text{A/cm}^2$, and $R_f(77\ \text{K}) = 0.228\ \text{m}\Omega\ \text{cm}^2$. The resistance values used in the calculations conform to the temperature dependence of the flux flow resistance in the form $R_f(T) = R_{f0}/[1 - (T/T_c)^2]$ [21], which is an approximation to the temperature dependence $R_f(T)$ obtained in [22, 23]. As is seen in Fig. 4, the theoretical dependences are in good agreement with the experimentally measured current–voltage characteristics of foamed BPSCCO at the initial part of the resistive transition.

The dependence of the differential resistance on the transport current is given by [24]

$$R_d = R_f\exp\left(-\left(\frac{2+D}{2}\right)^{\frac{2}{D}+1} i^{-\frac{2}{D}}\right). \quad (4)$$

Figure 5 presents theoretical curves calculated from Eq. (4) for the same parameter values as above. The resistance is proportional to the free vortex density n: $R_d = R_f(\Phi_0/B)n$, where $\Phi_0 \equiv hc/2e$ is the magnetic flux quantum, B is the magnetic field, h is Planck's constant, c is the speed of light, and e is the electron charge. A comparison of this expression and Eq. (4) shows that the free vortex density depends on the fractal dimension of the normal-phase clusters. The resistance of the superconductor is determined by the number of vortices broken away from pinning centers, since these vortices transfer the magnetic flux that induces the electric field. The more vortices are free to move, the stronger the induced electric field and, therefore, the higher the voltage across the sample at the same transport current.

The theoretical model of a superconductor containing fractal clusters of a normal phase adequately describes the experimental current–voltage characteristics in the region of the resistive transition. There is a deviation of the experimental curves from the calculated dependences for larger values of transport current. The reason for this discrepancy may be the change in the fractal dimension of cluster boundaries under the action of a large current, as well as the development of thermomagnetic instability.

4. CONCLUSIONS

Though different models, such as those developed in [21, 25, 26], can be used to describe the experimental current–voltage characteristics of polycrystalline HTS, the model of a superconductor with fractal clusters of a normal phase is best suited to superconducting foams, since this model reflects the actual structure of these materials and takes into account the influence of the structure parameters on the depinning critical current and current–voltage characteristics.

ACKNOWLEDGMENTS

The authors are grateful to A.D. Balaev for discussions of the results and to S.A. Satsuk for technical assistance.

This work was supported in part by a federal program for support of young scientists and scientific schools (grant MK 1682.2004.2), the Krasnoyarsk Regional Science Foundation (grant no. 12F0033C), and the St. Petersburg Science Center of the Russian Academy of Sciences.

REFERENCES

1. E. S. Reddy and G. J. Schmitz, Supercond. Sci. Technol. **15**, 21 (2002).
2. E. S. Reddy, M. Herweg, and G. J. Schmitz, Supercond. Sci. Technol. **16**, 608 (2003).
3. M. I. Petrov, T. N. Tetyueva, L. I. Kveglis, A. A. Efremov, G. M. Zeer, K. A. Shaihutdinov, D. A. Balaev, S. I. Popkov, and S. G. Ovchinnikov, Pis'ma Zh. Tekh. Fiz. **29** (23), 40 (2003) [Tech. Phys. Lett. **29**, 986 (2003)].
4. E. Bartolomé, X. Granados, T. Puig, X. Obradors, E. S. Reddy, and G. J. Schmitz, Phys. Rev. B: Condens. Matter **70**, 144 514 (2004).

5. E. Bartolomé, X. Granados, T. Puig, X. Obradors, S. Reddy, and J. Noudem, in *Proceedings of the International Applied Superconductivity Conference "ASC 2004," Jacksonville, FL, United States, 2004*, p. 52.
6. R. Zallen, Phys. Rev. B: Solid State **16**, 1426 (1977).
7. V. S. Kravchenko, A. I. Romanenko, O. G. Potapova, O. V. Razlevinskaya, and I. N. Kuropyatnik, Izv. Sib. Otd. Akad. Nauk SSSR, Ser. Khim. Nauk, No. 1, 85 (1990).
8. B. B. Mandelbrot, *Fractals: Form, Chance, and Dimension* (Freeman, San Francisco, 1977).
9. L. D. Landau and E. M. Lifshitz, *Course of Theoretical Physics*, Vol. 6: *Fluid Mechanics* (Nauka, Moscow, 1986; Pergamon, New York, 1987).
10. A. D. Balaev, Yu. V. Boyarshinov, M. M. Karpenko, and B. P. Khrustalev, Prib. Tekh. Eksp., No. 3, 167 (1985).
11. G. Blatter, M. V. Feigelman, V. B. Geshkenbein, A. I. Larkin, and V. M. Vinokur, Rev. Mod. Phys. **66**, 1125 (1994).
12. K. Yamafuji and T. Kiss, Physica C (Amsterdam) **258**, 197 (1996).
13. Yu. I. Kuzmin, Phys. Lett. A **267**, 66 (2000).
14. Yu. I. Kuzmin, Phys. Rev. B: Condens. Matter **64**, 094 519 (2001).
15. M. Ziese, Physica C (Amsterdam) **269**, 35 (1996).
16. M. Ziese, Phys. Rev. B: Condens. Matter **53**, 12422 (1996).
17. Yu. I. Kuzmin, Phys. Lett. A **281**, 39 (2001).
18. M. Prester, Phys. Rev. B: Condens. Matter **60**, 3100 (1999).
19. Yu. I. Kuzmin, Phys. Lett. A **300**, 510 (2002).
20. Yu. I. Kuzmin, J. Low Temp. Phys. **130**, 261 (2003).
21. A. Kilic, Supercond. Sci. Technol. **8**, 497 (1995).
22. J. Bardeen and M. J. Stephen, Phys. Rev. **140**, A1197 (1965).
23. J. Clem, Phys. Rev. Lett. **20**, 735 (1968).
24. Yu. I. Kuz'min, Pis'ma Zh. Tekh. Fiz. **30** (11), 29 (2004) [Tech. Phys. Lett. **30**, 457 (2004)].
25. R. Kümmel, U. Gunsenheimer, and R. Nicolsky, Phys. Rev. B: Condens. Matter **42**, 3992 (1990).
26. M. I. Petrov, D. M. Gokhfeld, D. A. Balaev, K. A. Shaihutdinov, and R. Kümmel, Physica C (Amsterdam) **408**, 620 (2004).

Translated by G. Tsydynzhapov